A VARIATIONAL MODEL OF DISJOINING PRESSURE: LIQUID FILM ON A NONPLANAR SURFACE

Dmitriy Silin[1*] and George Virnovsky[2]

[1]Lawrence Berkeley National Laboratory, University of California, Berkeley, CA

[2]International Research Institute of Stavanger AS, Stavanger, Norway

ABSTRACT. Variational methods have been successfully used in modelling thin liquid films in numerous theoretical studies of wettability. In this paper, the variational model of the disjoining pressure is extended to the general case of a two-dimensional solid surface. The Helmgoltz free energy functional depends both on the disjoining pressure isotherm and the shape of the solid surface. The augmented Young–Laplace equation (AYLE) is a nonlinear second-order partial differential equation. A number of solutions describing wetting films on spherical grains have been obtained. In the case of cylindrical films, the phase portrait technique describes the entire variety of mathematically feasible solutions. It turns out that a periodic solution, which would describe wave-like wetting films, does not satisfy the Jacobi's condition of the classical calculus of variations. Therefore, such a solution is nonphysical. The roughness of the solid surface significantly affects liquid film stability. AYLE solutions suggest that film rupture is more likely at a location where the pore-wall surface is most exposed into the pore space and the curvature is positive.

1. INTRODUCTION

Wettability is the property of solid materials to contact preferentially, one fluid relative to the other. Oil recovery mechanisms strongly depend on the wettability of the reservoir rock [1, 21, 23]. Many natural rocks are water-wet. In presence of oil and water, the molecular forces acting between the solid and the fluids in a thin water film on the solid surface develop a disjoining pressure. This disjoining pressure results from the interaction between the electrostatic double-layer and van der Waals forces. It is characterized by a disjoining pressure isotherm, which is affected by the temperature, chemical composition of the fluids, and the solid mineralogy [7, 9, 14, 15, 29, 34].

*****The final version of this work has been prepared by the first author after Dr. Virnovsky's sudden death on the 12th of March 2008, while visiting Lawrence Berkeley National Laboratory.

At a given temperature, the magnitude of the disjoining pressure depends on the thickness and the geometry of the film.

Stability of the water liquid film on the solid surface means that the latter remains water-wet. However, the reservoir evolution can create conditions for film rupture and creation of a direct contact between the oil and the solid. Consequently, the rock can become oil-wet, or mixed-wet. Water film stability under various temperature and salinity conditions has been the focus of a number of recent studies [13, 27, 28, 36]. In the laboratory, alteration of the wettability is modelled by ageing rock samples [21, 23, 27]. In enhanced oil recovery, wettability alteration is achieved by injection of a surfactant or steam.

A typical thickness of the liquid film is in the range of tens of nanometers. Therefore, the roughness of the solid surface or the smallness of the grains (as in chalk) also have an impact on the wettability alteration. Unlike the temperature and chemical composition of the reservoir fluids, the pore space geometry is hardly modifiable in an enhanced oil recovery project.

At thermodynamic equilibrium, the shape of the fluid-fluid interface and the thickness of the wetting fluid film can be described as a minimum of the Helmholtz free energy [7, 9, 15, 29, 34]. Mathematically, a small variation of an equilibrium configuration film can only increase the the value of the energy functional. The augmented Young–Laplace equation (AYLE) is a necessary condition for a minimum of the energy functional. If the fluid-fluid interface is far enough from the solid surface, the influence of the disjoining pressure vanishes and the AYLE reduces to the classical Young–Laplace equation.

The wettability can be quantified by the contact angle formed by the interface between two fluids at the solid surface. Assuming that the solid surface is ideally flat and that one of the main curvatures of the film surface is negligibly small relative to the other, Frumkin [10] and Derjagin [8] employed a variational approach to expressed the contact angle through the disjoining pressure isotherm.

This work presents a theoretical study of how the solid-surface geometry impacts the shape and stability of the thin liquid film. We assume that the chemical compositions of the fluids and the solid, as well as the temperature, are fixed. The new element here is the dependence of the energy functional on the shape the solid surface. We extend the variational model to the general case of a liquid film on a two-dimensional solid surface. We obtain analytical or semi-analytical solutions to the AYLE assuming simple geometric shapes of the underlying solid. Even such a simplified analysis provides valuable insights into how the roughness of the pore walls influences wettability alteration. Experimental

measurements of the disjoining pressure isotherm are very difficult and published data are sparse. In this study, we use the parameterized curves proposed by Yeh *et al.* [35].

In a general case, the AYLE is a nonlinear Laplace equation. However, a assumption of flat or cylindrical film geometry reduces the dimensionality of the problem and transforms the AYLE into a second-order ordinary differential equation (ODE). Several studies present a number of solutions to the ODE version of AYLE [16–20, 34, 35, 37, 38]. Rigorously speaking, a cylindrical film surface cannot be a least-energy surface [25]. However, the relative simplicity of the solution makes a cylindrical approximation reasonable if the contrast between the main curvatures of the fluid interface is large. This approximation has been extensively used in pore-network multiphase flow studies [3, 4, 24].

The AYLE is only a necessary condition for a weak minimum of the energy functional, so not every solution to the AYLE corresponds to a minimum of free energy. A solution, which does not correspond to a minimum of energy, is physically meaningless. We demonstrate that a periodic solution to AYLE describing a film surface in the form of periodical waves [29, 30] does not provide a local minimum to the energy functional since it does not satisfy the Jacobi's condition [11, 12]. Therefore, such a periodical solution is non-physical.

The paper is organized as follows. In Section 2, we present a general variational model of water film on a two-dimensional solid surface in space. The formulation employs the terminology of differential geometry, which is summarized in Appendix A. In Section 3, we consider films on cylindrical surfaces. Section 4 analyzes the variety of all solutions to an ODE version of AYLE using a phase portrait [26]. We demonstrate that the oscillating films fail to satisfy Jacobi condition for a minimum, which renders such solutions nonphysical. Appendix B summarizes the facts of the classical calculus of variations used in this study.

Gravity is neglected in all calculations.

2. A general variational model of the disjoining pressure

Away from the solid surface, the shape of the water-oil interface is determined by the interfacial tension and the capillary pressure. In such a case, the classical Young–Laplace equation provides a necessary condition of thermodynamic equilibrium. It assumes that the thickness of interface can be neglected. In fact, this interface is the transition zone between the two fluid phases and has a finite thickness. If the latter is comparable to the thickness of the liquid film on the solid

surface, then the zones of the interfacial forces acting at the solid-fluid and fluid-fluid interfaces overlap. This overlap generates additional forces increasing or decreasing the pressure inside the liquid film on the solid surface [9]. This pressure increment is called disjoining pressure.

At thermodynamic equilibrium, the shape of a thin liquid film between the solid surface and the nonwetting fluid phase is characterized by a local minimum of the Helmholtz free energy. This observation leads to a problem of the classical calculus of variations. The usual assumption is that the solid surface is ideally flat and that one of the main curvatures of the film surface is negligibly small relative to the other. In such a case, the variational problem is one-dimensional, and the AYLE, which is the Euler–Lagrange equation of the energy functional (see Appendix B for the terminology of the calculus of variations), is an ordinary differential equation. Numerous theoretical studies of wettability are based on this assumption [2, 6, 7, 16–19, 27, 29, 34, 35, 38].

The main objective of this section is to extend the one-dimensional variational model to a more general case of a thin film on a two-dimensional non-flat solid surface. The curvature of the solid surface is not too large, so that the assumption that the disjoining pressure, Π, is a function of the thickness of the film [9, 15], h, remains valid. The thickness of the film is the shortest distance between the film surface and the solid. Therefore, it is measured along the normal. A normal projection of a solid surface element of area dA on the film surface has a different area, $\Xi(h)dA$, which depends on the thickness of the film. Clearly, for any surface, $\Xi(h) = 1$ if $h = 0$. Moreover, for a uniform liquid film over a flat solid surface, $\Xi(h) = 1$ for all $h \geq 0$. For a uniform film on a spherical solid of radius R, one has $\Xi(h) = (1 + h/R)^2$. In general, the factor $\Xi(h)$ may also depend on the location on the surface (see Equation (54) in Appendix A).

The differential of the work of the disjoining pressure corresponding to an infinitesimal increment of the film thickness, dh, can be expressed through the variation of a disjoining pressure potential, P:

$$dP(h) = -\Pi(h)\Xi(h)\, dh \tag{1}$$

Note the factor $\Xi(h)$ accounting for the dependance of the surface area on the thickness of the film. The total work of the disjoining pressure on changing the thickness of the film is evaluated by the integral of the expression in Equation (1). A potential is determined up to a constant additive term. By putting the potential equal to zero at infinity, one obtains

$$P(h) = \int_h^\infty \Pi(\xi)\Xi(\xi)\, d\xi \tag{2}$$

The upper limit of integration is infinite for compatibility with the definition of the potential for a flat solid surface [9, 15]. Rigorously speaking, the normal directions of a non-convex solid surface intersect each other, which may lead to an ambiguity in Equation (2). Consequently, the definition of the potential in terms of differentials, Equation (1), rather than finite increments, is more general.

Consider a parametrization of a portion of the solid surface by a radius-vector $\mathbf{r} = \mathbf{r}(u, v)$, where the local coordinates u, v are bounded by a two-dimensional domain Ω. The integral

$$J[h] = \int_{\Omega} L(x, y, h, \nabla h)\, dudv \tag{3}$$

where

$$L\left(x, y, h, \nabla h\right) = \sigma\sqrt{EG - F^2} + \sqrt{E_0 G_0 - F_0^2}\left(\sigma_{\mathrm{SW}} - \sigma_{\mathrm{SO}} + P(h)\right) + p_c\sqrt{E_0 G_0 - F_0^2}\int_0^h \Xi(\xi) d\xi \tag{4}$$

evaluates the excess Helmholtz free energy in the water film over the corresponding portion of the solid surface. In Equation (4), p_c is the capillary pressure, and σ, σ_{SW}, and σ_{SO} are (respectively) the interfacial tension coefficients for water-oil, solid-water and solid-oil interfaces. The functions E_0, F_0, G_0, and E, F, and G characterize the solid surface and liquid film geometry – see Equations (38) and (51)–(53) in Appendix A. The first term on the right-hand side in Equation (4) accounts for the excess energy of the water-oil interface. The second term on the right is the sum of excess energy which is due to replacement of one fluid with another at the solid surface, and the disjoining pressure potential. The last term is the contribution of the capillary pressure, which is the difference between oil and water pressures. An equilibrium film configuration corresponds to a minimum of the excess energy functional in Equation (3). The Euler–Lagrange equation, a necessary condition for minimum, has the form:

$$\nabla \cdot \nabla_{\xi} L(x, y, h, \nabla h) - \frac{\partial L}{\partial h} = 0 \tag{5}$$

where ∇_{ξ} denotes the gradient of function L with respect to its fourth argument. If the film thickness at the boundary of the domain Ω is known, then one arrives at a Dirichlet boundary-value problem:

$$h|_{\partial\Omega} = h_0(x, y) \tag{6}$$

Equation (5) is a second-order nonlinear partial differential equation. It is the AYLE in the most general form. For a one-dimensional film on

a flat solid surface, Equation (5) reduces to the one-dimensional ODE version of AYLE presented *e.g.* in [29, 34].

Even for a relatively simple underlying solid surface, obtaining a solution to Equation (5) is difficult. As a compromise between complexity and generality, we consider an axisymmetric film on spherical grains. As an example, let us describe a film on a spherical surface as a solution to the AYLE.

Consider a spherical surface of radius R parameterized by u and v:

$$\mathbf{r}_0(u,v) = R\sin u\cos v\,\mathbf{i} + R\sin u\sin v\,\mathbf{j} + R\cos u\,\mathbf{k} \tag{7}$$

where $0 \le u \le \pi$, $0 \le v < 2\pi$, $\mathbf{r} = (x, y, z)$ is the radius-vector, and and $\mathbf{i}$, $\mathbf{j}$, and $\mathbf{k}$ are unit coordinate vectors. The outer unit normal vector is parameterized by

$$\mathbf{n} = \sin u\cos v\,\mathbf{i} + \sin u\sin v\,\mathbf{j} + \cos u\,\mathbf{k} = \frac{1}{R}\mathbf{r}_0(u,v) \tag{8}$$

Let $h = h(u, v)$ be the thickness of the liquid film measured in the direction of the normal to the solid surface. Then $\mathbf{r} = \mathbf{r}_0 + h\mathbf{n}$ parameterizes the surface of the film. Equivalently,

$$\mathbf{r}(u,v) = \left(1 + \frac{h}{R}\right)\mathbf{r}_0(u,v) \tag{9}$$

The elements of the first quadratic form on a sphere (see Equation (46), Appendix A) are

$$E_0 = R^2 \tag{10}$$

$$F_0 = 0 \tag{11}$$

$$G_0 = R^2\sin^2 u \tag{12}$$

For the surface of the film, using Equations (51)–(53) of Appendix A one obtains

$$E = (R+h)^2 + \frac{\partial h}{\partial u}^2 \tag{13}$$

$$F = \frac{\partial h}{\partial u}\frac{\partial h}{\partial v} \tag{14}$$

$$G = (R+h)^2\sin^2 u + \frac{\partial h}{\partial v}^2 \tag{15}$$

For an axisymmetric film, the thickness h is a function of u only. Hence, the derivative $\dfrac{\partial h}{\partial v}$ vanishes. Therefore, $F = 0$, and, by virtue of Equation (56) of Appendix A, the film surface area and volume differentials

are

$$dA = (R+h)\sin u\sqrt{\left(\frac{\partial h}{\partial u}\right)^2 + (R+h)^2}\,dudv \tag{16}$$

$$dV = \frac{1}{3}\left[(R+h)^3 - R^3\right]\sin u\,dudv \tag{17}$$

Let us introduce a dimensionless film thickness

$$\eta(u) = \frac{h(u)}{R} \tag{18}$$

After cancelling a common factor of $2\pi R^2$, the integral energy functional becomes equal to

$$J[\eta] = \int_{u_0}^{u_1} L\left(u, \eta(u), \frac{d\eta(u)}{du}\right)\,du \tag{19}$$

where

$$L(u,\eta,\xi) = \Big[\sigma(1+\eta)\sqrt{\xi^2+(1+\eta)^2} + \sigma_{\mathrm{SW}} - \sigma_{\mathrm{SO}} + P_R(\eta R) + \frac{1}{3}p_c\left[(1+\eta)^3 - 1\right]R\Big]\sin u \tag{20}$$

By virtue of Equation (56) of Appendix A, the disjoining pressure potential is defined as

$$P_R(h) = \int_h^\infty \Pi(\zeta)\left(1+\frac{\zeta}{R}\right)^2 d\zeta \tag{21}$$

The augmented Young–Laplace equation takes on the following form:

$$\sigma\frac{\eta''(1+\eta)^3 - 3\eta'^2(1+\eta)^2 - 2(1+\eta)^4}{\left(\eta'^2+(1+\eta)^2\right)^{3/2}} + \sigma\frac{(1+\eta)\eta'}{\sqrt{\xi^2+(1+\eta)^2}}\cot u + \Pi(\eta R)\,(1+\eta)^2\,R - p_c(1+\eta)^2 R = 0 \tag{22}$$

For a uniform film, the derivatives vanish and one obtains

$$-\frac{2\sigma}{(1+\eta)R} = p_c - \Pi(\eta R) \tag{23}$$

Figure 1 shows an example of a liquid bridge at a grain-to-grain contact calculated by solving Equation (22). As the boundary condition, common for both solutions, we have used the thickness of the film at the junction point, and the fact that the tangential plane to the film at the junction is parallel to the line connecting the centers.

Figure 2 shows another solution to AYLE: a bubble at a contact with a solid spherical grain, deformed by the disjoining pressure. The AYLE

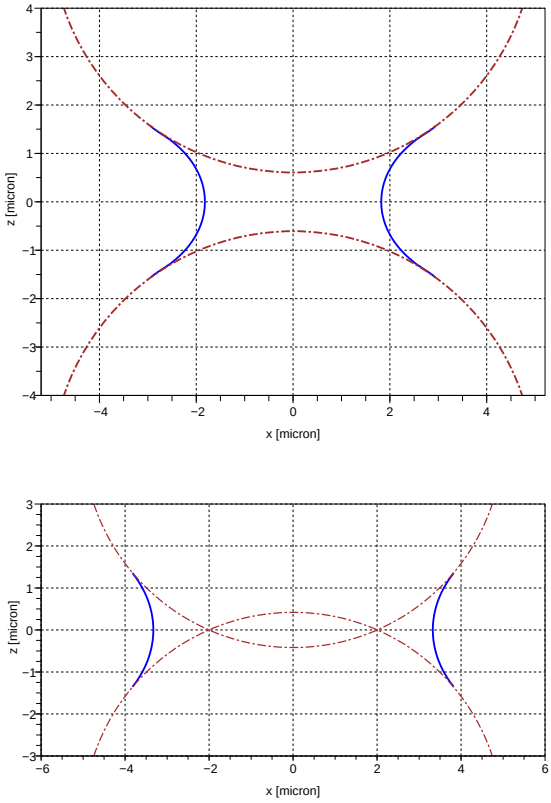

FIGURE 1. Two examples of a liquid bridge between two spherical grains: most of the film is controlled by the surface tension.

equation is solved for each grain individually. As the boundary conditions, we have used the minimal film thickness and the zero derivative of the thickness at minimum. Although a sphere is the most symmetric ideal geometric shape, its parametrization, Equation (7), includes two poles: $u = 0$ and $u = \pi$. At these poles, the cotangent function in Equation (22) blows up into infinity. However, this singularity can be resolved in the following way. An axisymmetric solution must satisfy the condition $\eta'(0) = 0$ at both poles. Thus, the Taylor expansion of $\eta(u)$ near each pole skips the linear term. For example, at the pole $u = 0$:

$$\eta(u) = \eta(0) + \alpha u^2 + o(u^2) \tag{24}$$

where $\alpha = 0.5\eta''(0)$. Let us express α through the dimensionless thickness of the film at the pole, $\eta(0)$. By substituting this expression into

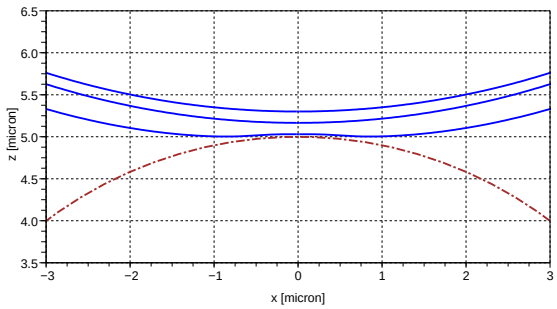

FIGURE 2. Deformation of a bubble by a spherical grain.

Equation (22) and by passing to the limit as $u \to 0$, one obtains

$$\sigma \frac{2\alpha(1+\eta(0))^3 - 2(1+\eta(0))^4}{((1+\eta(0))^2)^{3/2}} + (\Pi(\eta(0)R) - p_c)\,(1+\eta(0))^2\,R = 0 \tag{25}$$

Consequently,

$$\alpha = 1 + \eta(0) + \frac{R(p_c - \Pi(\eta(0)R))}{2\sigma}(1+\eta(0))^2 \tag{26}$$

Equations (24) and (26), valid for a small u, determine the thickness of the film near the pole. Each solution shown in Figure 2 has been obtained as an extension of this asymptotic solution by solving the AYLE Equation (22).

3. A variational model of a film on a round cylindrical surface

In this section, we assume that the solid surface is cylindrical. It means that one of the main curvatures is much smaller than the other one and can be assumed to be equal zero. Let the axis of a solid cylinder of radius R be aligned with the coordinate z in a Cartesian coordinate system x, y, z. The surface of this cylinder can be parameterized by the equation

$$(x_0(u), y_0(u)) = R(\cos u, \sin u), \quad 0 \le u < 2\pi \tag{27}$$

Water forms a film covering (may be, only partially) the surface of the solid. Oil fills the space outside the cylinder beyond this film. Denote by $h = h(u)$ the film thickness in the radial direction. Then, the equation

$$(x(u), y(u)) = (R + h(u))(\cos u, \sin u) \tag{28}$$

parameterizes the water-oil interface (Figure 3).

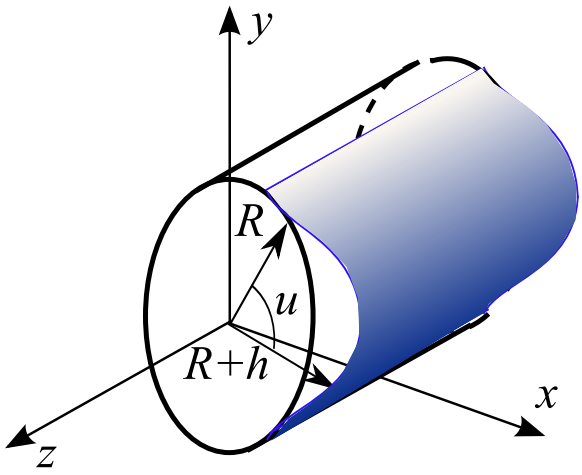

FIGURE 3. A liquid film on a cylindrical surface

Assume that the water film covers the entire solid surface of the cylinder between the bounding angles u_1 and u_2. Then, by virtue of Equations (3)–(4), the excess Helmholtz free energy functional has the form:

$$J[h] = \pi \int_{u_1}^{u_2} \left\{ \sigma \sqrt{\left[R + h(u)\right]^2 + h'(u)^2} + \left[\sigma_{\rm SW} - \sigma_{\rm SO} + P_R(h)\right] R \right. \\ \left. + \frac{1}{2} p_c \left[(R+h)^2 - R^2\right] \right\} du \quad (29)$$

Note that the boundaries, u_1 and u_2, are not necessarily fixed. From Equations (2) and (55), the disjoining pressure potential, $P_R(h)$, is defined through the disjoining pressure Π by the equation

$$P_R(h) = \int_h^\infty \Pi(\xi) \left(1 + \frac{\xi}{R}\right) d\xi \quad (30)$$

At $R \to \infty$, this formula reduces to the expression for the disjoining pressure potential for a flat solid surface, $P(h)$, defined in [7, 29, 34]. After dividing by πR, Equation (29) takes on the form

$$J[\eta] = \int_{u_1}^{u_2} \left\{ \sigma \sqrt{\left(1 + \eta\right)^2 + (\eta')^2} + \sigma_{\rm SW} - \sigma_{\rm SO} + P_R(\eta R) \right. \\ \left. + \frac{1}{2} p_c (\eta^2 + 2\eta) R \right\} du \quad (31)$$

The Euler–Lagrange equation for this integral functional is

$$\frac{\sigma}{R}\frac{\eta''(1+\eta)-2\eta'^2-(1+\eta)^2}{\left[(1+\eta)^2+\eta'^2\right]^{3/2}}+\Pi(R\eta)-p_c=0 \tag{32}$$

which is the AYLE for a cylindrical interface. For a uniform thickness film, $h(u)=Const$, Equation (32) yields

$$\Pi(h)=p_c+\frac{\sigma}{R+h} \tag{33}$$

Since the integrand in Equation (31) does not depend explicitly on the angle u, the order of the Euler–Lagrange equation can be reduced [11, 12]:

$$\sigma\frac{(1+\eta)^2}{\sqrt{(1+\eta)^2+(\eta')^2}}+\sigma_{\mathrm{SW}}-\sigma_{\mathrm{SO}}+P_R(\eta R)+\frac{1}{2}p_c(\eta^2+2\eta)R=C \tag{34}$$

The constant C must be determined from the boundary conditions. For example, if the boundary conditions include a known thickness of the film, say, at $u=u_2$, but the angle u_2 is not fixed, then the transversality condition (see Equation (63) in Appendix B) yields $C=0$. By making η an independent variable, the first-order ODE (34) can be integrated explicitly, and the solution can be obtained in the form $u=u(\eta)$.

Figure 4 illustrates the qualitative difference between the liquid films on flat and non-flat surfaces. It shows an example of a disjoining pressure isotherm based on parametrization from [34] plotted versus the thickness of the film, along with the right-hand side of Equation (33), and a similar expression for a surface of negative curvature (the inner surface of a cylinder). The top dashed line plots the difference between the capillary pressure and the surface tension versus the film thickness h for a film on the outer surface of a cylinder. The dashed line in the middle is the capillary pressure for a uniform liquid film on a flat surface. Finally, the bottom dashed curve is the difference between the capillary pressure and the surface tension versus h for a liquid film on the inner surface of a cylinder. This curve is plotted just to illustrate the role of the sign of the solid surface curvature. The difference between the flat and cylindrical cases is that in the latter, the curvature of the solid surface explicitly enters the equations.

4. The phase portrait of AYLA for a cylindrical surface

The input data for solving AYLE are subject to uncertainty. Therefore, a qualitative description of the entire variety of all possible solutions can be very helpful for describing all feasible geometries of liquid

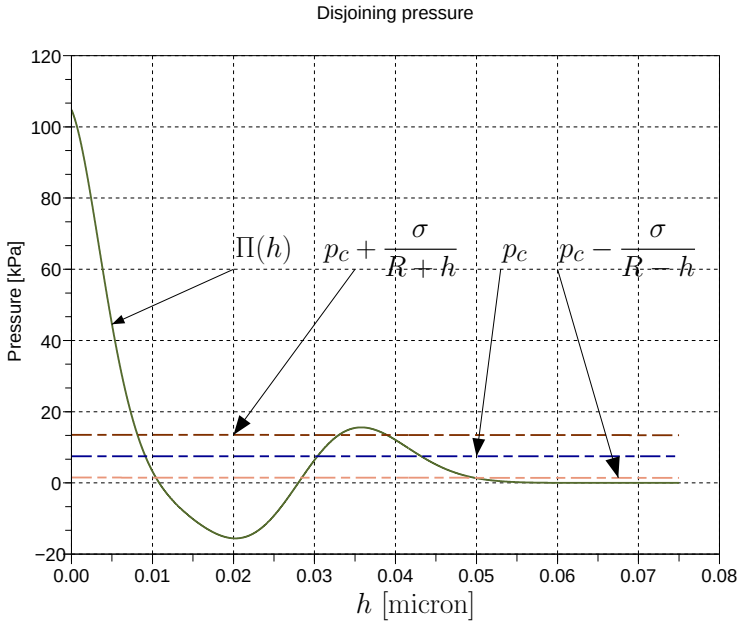

FIGURE 4. The disjoining pressure $\Pi(h)$, capillary pressure p_c, and the hyperbolas $p_c + \dfrac{\sigma}{R+h}$ and $p_c - \dfrac{\sigma}{R-h}$ corresponding to the liquid films on the surfaces of a grain and pore, respectively, plotted against the thickness of the film, h.

films. To obtain such a description, we employ the phase portrait of a second-order dynamic system [26], focusing on the cylindrical approximation, Equation (32). The variables

$$\zeta_1(u) = \eta(u) \text{ and } \zeta_2(u) = \eta'(u) \tag{35}$$

transform the single second-order ordinary differential equation (32) into an equivalent nonlinear system of two first-order ordinary differential equations

$$\begin{cases} \zeta_1' &= \zeta_2 \\ \zeta_2' &= \dfrac{1}{1+\zeta_1}\left[2\zeta_2^2 + (1+\zeta_1)^2 + \dfrac{R}{\sigma}(p_c - \Pi(R\eta))\left(\zeta_2^2 + (1+\zeta_1)^2\right)^{3/2}\right] \end{cases} \tag{36}$$

A solution plotted in a coordinates ζ_1, ζ_2 phase plane is called a trajectory [26] of the system defined by Equation (36). The phase portrait is the variety of all trajectories [26]. By virtue of Equation (35), a phase portrait shows the relationship between η and η'. For example, a

constant-thickness film, $\eta(u) \equiv \eta_0$, is displayed as a single point $(\eta_0, 0)$, called an equilibrium point of the system (36). The corresponding solution in the form $\eta = \eta(u)$ plotted versus u is a straight line parallel to the axis u. A periodic trajectory is called a cycle and is displayed in the phase portrait as a loop. A cycle describes a wave-like surface.

Figure 5 displays the phase portrait of the system described by Equation (36). The arrows show the vector field defined by the right-hand side. The large dots A, B, and C show three equilibrium points, which are constant-thickness solutions $\eta(u) = \text{Const}$. These three points, in turn, correspond to the three intersections of the disjoining pressure curve and the hyperbola $p(h) = p_c + \dfrac{\sigma}{R+h}$ (Figure 4). The entire classification of equilibrium points includes a focus, a node, a saddle point, and a center [26]. In Figure 5, the points A and C are saddle points, whereas the point B is a center. No phase trajectory can reach an equilibrium point on a finite interval u. This means that either the entire solution corresponds to a constant-thickness film, or the thickness cannot be constant on a nonzero interval. A solution to the system (36) may approach a constant-thickness solution asymptotically, but the two can never partially coincide. This fact of the classical theory of ordinary differential equations is in contradiction with the conclusion derived in [17], where some solutions are partially constant-thickness and partially not.

Some phase trajectories crossing the abscissa to the right of the equilibrium point A are cycles, some are not. Figure 6 shows a few examples of the noncycling trajectories plotted in a coordinate plane x, y. The shape of the water-oil interface resembles a deformed bubble of oil. In particular, one observes an alteration of the sign of the curvature due to the interaction between disjoining pressure and surface tension. The farther from the solid the interface is, the more the bubble shape is close to circular.

The film shapes corresponding to the trajectories crossing the abscissa to the left from point A look like droplets. The corresponding thickness of the film is smaller than that of the uniform film corresponding to point A. Such nanodroplets, which have flat pancake shapes, have been discussed in [5] from the standpoint of the Derjaguin, Landau, Verwey and Overbeek (DLVO) theory. Tyrrell and Attard [32] experimentally observed nanobubbles using atomic-force microscopy.

One interesting type of trajectories is the cycles near point B (Figure 5). Each cycle corresponds to a wave-like surface of the liquid film, Figure 7. The existence of oscillating periodic solutions to the AYLE in the case of a flat solid surface has been mentioned in [29]. However,

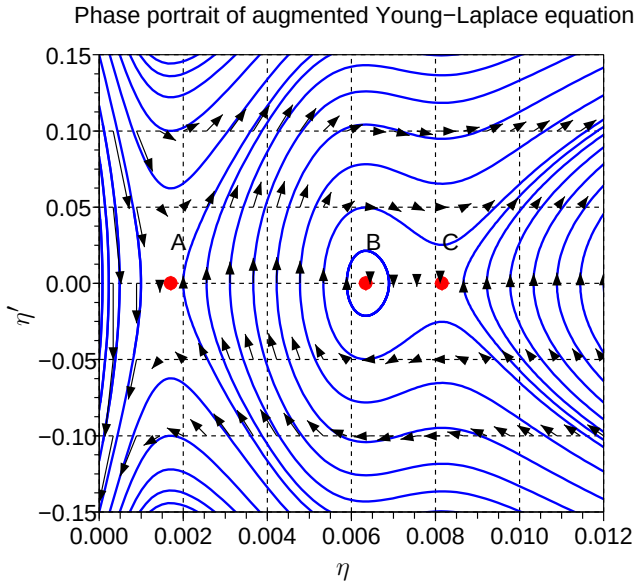

FIGURE 5. The phase portrait of the system (36) for $\sigma = 30 \times 10^{-3}$ N/m, $p_c = 6$ kPa, and the radius $R = 5$ μm.

as is demonstrated in Appendix B, such a profile does not satisfy the Jacobi's condition. Therefore, a periodic solution does not provide a local minimum of the energy functional and is non-physical.

At a negative capillary pressure, the phase portrait may significantly depend on the dimensionless group $P_c R/\sigma$. For some values, it may include only two equilibrium points: the saddle point, corresponding to the broken film, and the center, corresponding to the periodically oscillating solutions (Figure 8). An oscillating solution does not minimize the energy functional and does not describe a physically feasible liquid film. If the radius of the solid surface is small enough, there can be an intermediate region where the shape of the film is determined mostly by the interaction between surface tension and disjoining pressure. The disjoining pressure prevails in very thin films. In Figures 5 and 8, the parts of the phase portraits corresponding to $\eta < 0.002$ are similar for both positive and negative capillary pressures. In both cases, the trajectories correspond to nanodroplets. The noncycling trajectories crossing the abscissa to the right from point B in Figure 8 describe droplets on the cylinder surface.

Figure 9 shows a calculated film profile for a rough surface, where the roughness is modeled as a sequence of round bumps. This solution to

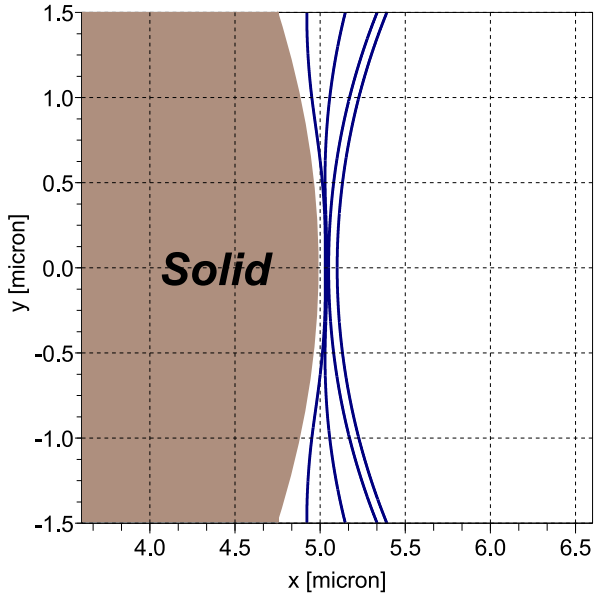

FIGURE 6. A circular bubble of oil deformed by disjoining pressure. The rightmost film profile is practically undistorted bubble whose round shape is determined by the capillary pressure and surface tension. Note the change of the sign of the curvature.

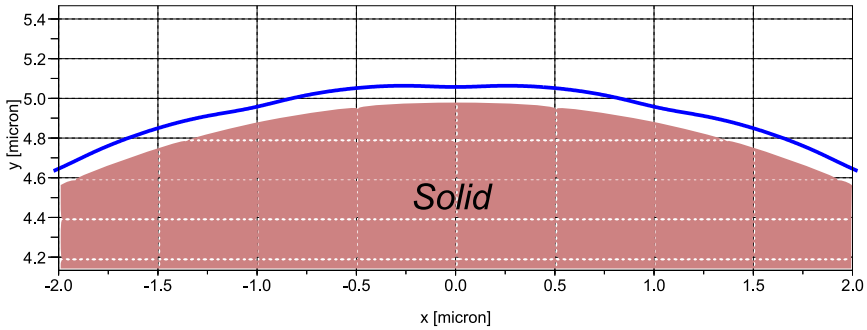

FIGURE 7. A periodically oscillating solution to the AYLE. The amplitude of the thickness variation has been amplified for visualization.

the AYLE is composed of several segments, each of which corresponds to a single grain. The junction between any two adjacent segments is at the midpoint between the centers of the grains. Boundary conditions at each junction point impose a smooth transition between the segments. Figure 9 shows that the locations of most likely film rupture are at the tops of the grains, where the film is the thinnest. Since the curvature of

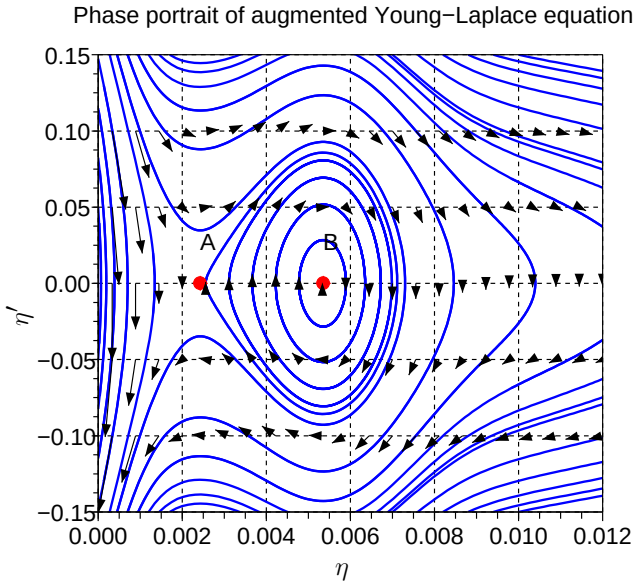

FIGURE 8. The phase portrait for a negative capillary pressure: $p_c = -10$ kPa, $R = 5$ μm.

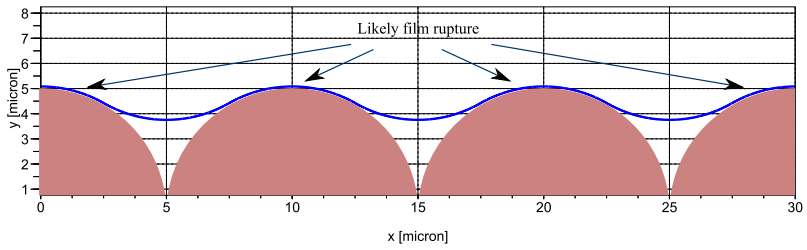

FIGURE 9. A liquid film on a rough surface.

the surface of each bump is constant, we conclude that the local shape of the surface does not solely determine the stability of the film.

5. Summary and conclusions

Variational methods have been successfully used in wettability studies over past few decades. At equilibrium, the shape of a thin water film on a water-wet solid surface corresponds to a minimum of the Helmholtz free energy of the system. The energy functional includes three components – the surface tension energy, the work of the capillary pressure, and the work of disjoining pressure in the form of an

increment of the potential. The film surface is characterized by an advanced Young–Laplace equation, which generalizes the classical Young–Laplace equation to account for the disjoining pressure. The latter is a result of interaction between molecular electrostatic double-layer and van der Waals forces. The presence of the disjoining pressure may result in an alteration in the sign of the water-oil interface curvature without changing the sign of the capillary pressure. A number of solutions to the AYLE reported in the literature are valid under the assumption that both the liquid film and the solid surface are cylindrical, *i.e.*, invariant with respect to a translation parallel to one of the coordinate axes. The present work has extended the variational approach to films on arbitrary solid surfaces. This extension in particular has required a modification of the disjoining pressure potential definition. Besides the disjoining pressure isotherm, the new definition explicitly involves the shape of the underlying solid surface.

The general AYLE is a nonlinear second-order partial differential equation. We have obtained a number of solutions characterizing axisymmetric liquid films on spherical surfaces and films at the contact areas between spherical grains.

For a cylindrical liquid film on a cylindrical solid surface, the AYLE reduces to a second-order ordinary differential equation. The entire variety of solutions has been characterized using the phase-portrait technique. For example, the equilibrium points characterize constant-thickness liquid films.

Not every solution to the AYLE necessarily provides a minimum to the energy functional. We have demonstrated that the periodic solutions, which would describe wave-shaped liquid film surfaces, fail the Jacobi's condition of the classical calculus of variations and therefore are nonphysical.

Alteration of the wettability involves, in particular, destabilization and a rupture of the liquid film. Calculations based on the AYLE show that the roughness of the solid surface significantly affects liquid film stability. Breakage in the film is more likely to occur at the most exposed parts of the solid surface having a positive curvature. To arrive at this conclusion, a solution to the AYLE has been obtained for a film on a regular pack of cylindrical grains of equal radii. Although the results of this work are basic and qualitative, they provide valuable insights into the role of disjoining pressure and the impact of the solid surface roughness on the mechanisms of wettability alteration.

(

Acknowledgement)

Most part of this study has been performed at International Research Institute of Stavanger (IRIS), Norway. The Research Council of Norway, ConocoPhillips and the Ekofisk Coventurers, including TOTAL, ENI, StatoilHydro and Petoro, have supported this work through the research center COREC. The first author greatly appreciates the hospitality of IRIS during his visit. Part of this work has been done at Lawrence Berkeley National Laboratory (LBNL) of the U.S. Department of Energy under Contract No. DE-AC02-05CH11231.

Dr. Andrea Cortis of LBNL and Mr. Olav Inge Frette of IRIS have read the manuscript and provided valuable remarks and recommendations, which are greatly appreciated. Many thanks to the anonymous reviewers for their careful reading of the manuscript and numerous suggestions.

Appendix A. Differential geometry

In this Appendix, we briefly summarize the concepts and facts of the differential geometry used in this study.

A.1. **Basic definitions.** Let a surface in 3D space be parameterized by two parameters, u and v:

$$\mathbf{r}_0(u,v) = X(u,v)\mathbf{i} + Y(u,v)\mathbf{j} + Z(u,v)\mathbf{k} \tag{37}$$

where $\mathbf{r}_0(u,v)$ is the radius-vector and $\mathbf{i}$, $\mathbf{j}$, and $\mathbf{k}$ are the vectors of an orthonormal basis. The geometry of the surface can be expressed through the so-called first quadratic form. The entries of this form are defined pointwise, through the derivatives of the radius-vector

$$E_0 = \frac{\partial \mathbf{r}_0}{\partial u}\cdot\frac{\partial \mathbf{r}_0}{\partial u}, \quad F_0 = \frac{\partial \mathbf{r}_0}{\partial u}\cdot\frac{\partial \mathbf{r}_0}{\partial v}, \text{ and } G_0 = \frac{\partial \mathbf{r}_0}{\partial v}\cdot\frac{\partial \mathbf{r}_0}{\partial v} \tag{38}$$

An elementary surface area can be expressed as

$$dA_0 = \sqrt{E_0G_0 - F_0^2}\,dudv \tag{39}$$

The unit normal vector at a point $\mathbf{r}_0(u,v)$ can be determined from the relationship

$$\mathbf{n}(u,v) = \pm\frac{\dfrac{\partial \mathbf{r}_0}{\partial u}\times\dfrac{\partial \mathbf{r}_0}{\partial v}}{\sqrt{E_0G_0 - F_0^2}} \tag{40}$$

where $\|\cdot\|$ denotes the Euclidean norm. The sign in the last equation is subject to the orientation convention. Both partial derivatives of the

normal vector with respect to u and v are tangential to the surface. Therefore, they can be expressed as

$$\begin{aligned}\frac{\partial \mathbf{n}}{\partial u} =& W_{11}(u,v)\frac{\partial \mathbf{r}_0}{\partial u} + W_{12}(u,v)\frac{\partial \mathbf{r}_0}{\partial v}\\ \frac{\partial \mathbf{n}}{\partial v} =& W_{12}(u,v)\frac{\partial \mathbf{r}_0}{\partial u} + W_{22}(u,v)\frac{\partial \mathbf{r}_0}{\partial v}\end{aligned} \tag{41}$$

The symmetric matrix of coefficients $\{W_{ij}(u,v)\}$ is called the Weingarten mapping of the surface $\mathbf{r} = \mathbf{r}_0(u,v)$ [31]. The eigenvalues of this matrix are the main curvatures of the surface.

For a cylindrical surface, $\mathbf{r}_0(u,v) = (x(u), y(u), v)$, where $0 \le u < 2\pi$, one obtains

$$E_0 = \left(x'^2(u) + y'^2(u)\right),\ F_0 = 0,\ G_0 = 1,\ \text{ and }\ \mathbf{n}(u,v) = \frac{1}{\sqrt{x'^2(u) + y'^2(u)}}(-y'(u), x'(u), 0) \tag{42}$$

The matrix $W(u,v)$ has two eigenvalues:

$$\kappa = \frac{y''x' - y'x''}{\left(x'^2(u) + y'^2(u)\right)^{\frac{3}{2}}} \tag{43}$$

which is the curvature of the curve $(x(u), u(u))$, and zero. The surface area element is equal to

$$dA_0 = \sqrt{x'^2(u) + y'^2(u)}dudv \tag{44}$$

For a sphere of radius R centered in the origin,

$$\mathbf{r}_0(u,v) = R\left(\sin u\cos v\mathbf{i} + \sin u\sin v\mathbf{j} + \cos u\mathbf{k}\right) \tag{45}$$

where $0 \le u \le \pi$ and $0 \le v < 2\pi$, the elements of the first quadratic form and the unit normal vector are

$$E_0 = R^2, \qquad F_0 = 0, \qquad G_0 = R^2\sin^2 u, \qquad \text{and} \qquad \mathbf{n} = \sin u\cos v\mathbf{i} + \sin u\sin v\mathbf{j} + \cos u\mathbf{k} \tag{46}$$

The surface area element and the Weingarten matrix are equal to

$$dA_0 = R^2\sin u dudv \qquad \text{and} \qquad W = \frac{1}{R}I \tag{47}$$

where I is an identity matrix. Thus, both main curvatures of a sphere are reciprocal to the radius.

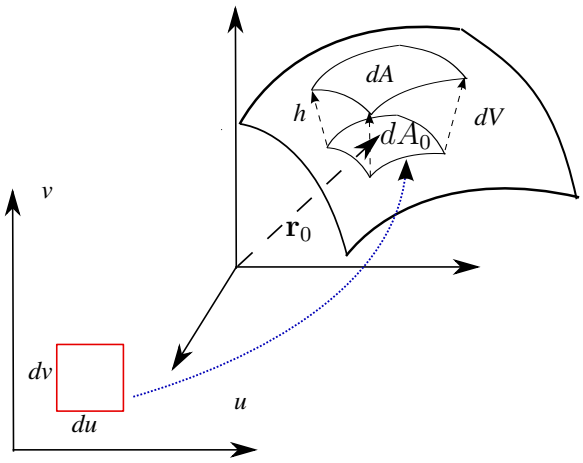

FIGURE 10. Mapping $u, v \to \mathbf{r}_0(u, v)$ and surface variation in the normal direction.

A.2. **Surface variations.** Let the surface parameterized by Equation (37) be perturbed in the normal direction. Then, for the perturbed surface,

$$\mathbf{r}(u, v) = \mathbf{r}_0(u, v) + h(u, v)\mathbf{n}(u, v) \tag{48}$$

Here $\mathbf{n}(u, v)$ is the normal unit vector and $h(u, v)$ is the magnitude of the perturbation (Figure 10). We will assume that $h(u, v) > 0$. We will also assume that the perturbed surface is smooth and has no self-intersections. From Equation (41),

$$\frac{\partial \mathbf{r}(u,v)}{\partial u} = \frac{\partial \mathbf{r}_0(u,v)}{\partial u} + \frac{\partial h(u,v)}{\partial u}\mathbf{n}(u,v) + h(u,v)W(u,v)\frac{\partial \mathbf{r}(u,v)}{\partial u} \tag{49}$$

$$\frac{\partial \mathbf{r}(u,v)}{\partial v} = \frac{\partial \mathbf{r}_0(u,v)}{\partial v} + \frac{\partial h(u,v)}{\partial v}\mathbf{n}(u,v) + h(u,v)W(u,v)\frac{\partial \mathbf{r}(u,v)}{\partial v} \tag{50}$$

For the elements of the first quadratic form for perturbed surface, one obtains

$$E = \left((I + hW)\frac{\partial \mathbf{r}_0}{\partial u}\right) \cdot \left((I + hW)\frac{\partial \mathbf{r}_0}{\partial u}\right) + \left(\frac{\partial h}{\partial u}\right)^2 \tag{51}$$

$$F = \left((I + hW)\frac{\partial \mathbf{r}_0}{\partial u}\right) \cdot \left((I + hW)\frac{\partial \mathbf{r}_0}{\partial v}\right) + \frac{\partial h}{\partial u}\frac{\partial h}{\partial v} \tag{52}$$

$$G = \left((I + hW)\frac{\partial \mathbf{r}_0}{\partial v}\right) \cdot \left((I + hW)\frac{\partial \mathbf{r}_0}{\partial v}\right) + \left(\frac{\partial h}{\partial v}\right)^2 \tag{53}$$

Denote by $dA(h)$ the elementary surface area of the perturbed surface evaluated for a constant h. Let us evaluate the correcting factor $\Xi(h)$ defined by the relationship: $dA(h) = \Xi(h)\, dA_0$. Straightforward, but

lengthy, calculations yield

$$\Xi(h) = \left\{ \left[\frac{\partial \mathbf{r}_0}{\partial u} \cdot (I + hW)^2 \left(\frac{\partial \mathbf{r}_0}{\partial u} \right) \right] \left[\frac{\partial \mathbf{r}_0}{\partial v} \cdot (I + hW)^2 \left(\frac{\partial \mathbf{r}_0}{\partial v} \right) \right] - \left[\frac{\partial \mathbf{r}_0}{\partial u} \cdot \left((I + hW)^2 \frac{\partial \mathbf{r}_0}{\partial v} \right) \right]^2 \right\}^{1/2} \Bigg/ \sqrt{E_0 G_0 - F_0^2} \quad (54)$$

For example, for a round cylindrical surface of radius R,

$$\Xi(h) = 1 + \frac{h}{R} \quad \text{and} \quad dA(h) = \left(1 + \frac{h}{R} \right) dA_0 \quad (55)$$

For a spherical surface of radius R, one obtains

$$\Xi(h) = \left(1 + \frac{h}{R} \right)^2 \quad \text{and} \quad dA(h) = \left(1 + \frac{h}{R} \right)^2 dA_0 \quad (56)$$

For a volume element between the original and perturbed surface, one obtains

$$dV(h) = \int_0^h d\Xi(\xi) d\xi \, du dv \quad (57)$$

Appendix B. Calculus of variations

Numerous models in mechanics, physics, and engineering can be formulated in a variational form, where the solution is a minimum of an energy functional [22, 33]. Here, we briefly review some concepts and results of the classical calculus of variations used in this study.

Let $\eta(u)$ be a smooth function defined on an interval $[u_1, u_2]$ and $L(u, \eta, \xi)$ be a smooth function of three variables. The variables are not necessarily scalar. Put

$$J[\eta] = \int_{u_1}^{u_2} L(u, \eta(u), \eta'(u)) \, dx \quad (58)$$

The objective is is to find an admissible curve $z = \eta(u)$ providing a minimum of the functional defined by Equation (58). The set of admissible curves may consist, for example, of all smooth functions $\eta(u)$ satisfying Dirichlet boundary conditions:

$$\eta(u_1) = \eta_1, \quad \eta(u_2) = \eta_2 \quad (59)$$

A function $\eta(u)$ is a *weak local minimum* of the functional (58) if $J[\eta]$ is the least value of the integral for all admissible curves, which only slightly differ from the curve $\eta(u)$ both by the value and by the derivative. If a curve $\eta(u)$ is a local weak minimum of the functional (58),

then it satisfies the Euler–Lagrange equation

$$\frac{d}{du}\,\frac{\partial}{\partial\xi}L(u,\eta(u),\xi)\bigg|_{\xi=\eta'(u)} - \frac{\partial}{\partial\eta}L(u,\eta,\eta'(u))\bigg|_{\eta=\eta(u)} = 0 \tag{60}$$

In general, the Euler–Lagrange equation is a second-order differential equation. Its solutions are called *extremals*. In many cases, the boundary conditions (59) determined a unique extremal. If the integrand does not depend explicitly on the first argument, $L(u,\eta,\xi) = L(\eta,\xi)$, then Equation (60) is equivalent to

$$\eta'(u)\,\frac{\partial}{\partial\xi}L(\eta(u),\xi)\bigg|_{\xi=\eta'(u)} - L(\eta(u),\eta'(u)) = C \tag{61}$$

The latter is a first-order differential equation involving a constant C. A solution and constant C can be determined from the boundary conditions, Equation (59).

The classical calculus of variations also considers problems, in which the endpoints of an admissible curve are not fixed by the boundary conditions (59), but are constrained by a curve or, perhaps, are not constrained at all. In such a case, the Euler–Lagrange equation is complemented with *transversality* conditions. For example, if the right-end point is constrained by the equation $\eta(u_2) = \psi(u_2)$, where ψ is a known function, then the respective transversality condition has the following form:

$$[\eta'(u_2) - \psi'(u_2)]\,\frac{\partial}{\partial\xi}L(\eta(u_2),\xi)\bigg|_{\xi=\eta'(u_2)} - L(\eta(u_2),\eta'(u_2)) = 0 \tag{62}$$

If $\psi(u) = \text{Const}$, then the value of an admissible curve, $\eta(u_2)$, is fixed, whereas the end of the interval, u_2, is not. In such a case, Equation (62) reads:

$$\eta'(u_2)\,\frac{\partial}{\partial\xi}L(\eta(u_2),\xi)\bigg|_{\xi=\eta'(u_2)} - L(\eta(u_2),\eta'(u_2)) = 0 \tag{63}$$

In particular, this transversality condition implies a zero constant C on the right-hand side of the reduced-order differential equation (61).

The Euler–Lagrange equation provides only a first-order *necessary* condition for a local minimum [11, 12]. Not every extremal provides a minimum or maximum of the functional. Additional criteria may be needed to figure out whether a given solution to the Euler–Lagrange equation is indeed a minimum of a functional. For example, the problem of the shortest path connecting two distinct points on a sphere can be formulated as a problem of calculus of variations. It can be demonstrated that any arc of a circle, which is the intersection of the spherical

surface and a plane passing through the center, is an extremal. Any two distinct points on a spherical surface can be connected by two such arcs. However, unless these two points are polar-opposite, only one of these arcs is the shortest connection.

In this section, we formulate second-order conditions by Jacobi and Legendre, which help to filter out extremals not providing a minimum to the functional. Moreover, the Jacobi's condition in conjunction with the strengthened Legendre condition is sufficient for a minimum of the functional [11, 12].

First, based on the integral functional (58), we define two functions

$$S(u) = \frac{1}{2}\frac{\partial^2 L}{\partial \xi^2} \text{ and } Q(u) = \frac{1}{2}\left(\frac{\partial^2 L}{\partial u^2} - \frac{d}{dx}\frac{\partial^2 L}{\partial u \partial \xi}\right) \tag{64}$$

Here, the expressions are evaluated at $\eta = \eta(u)$ and $\xi = \eta'(u)$. The second-order linear differential equation

$$-\frac{d}{du}\left(S\chi'\right) + Q\chi = 0 \tag{65}$$

where $\chi = \chi(u)$ is the unknown function, is called the Jacobi equation. A value $\widetilde{u}$, $u_1 < \widetilde{u} < u_2$, is called a conjugate point if there exists a nonzero solution to Equation (65), such that $\chi(u_1) = \chi(\widetilde{u}) = 0$. The necessary Jacobi condition says that if $\eta(u)$ provides a minimum to the integral functional (58), then there exists no conjugate point on the interval u_1, u_2. In addition to the Jacobi necessary condition, an extremal $\eta(u)$ providing a minimum satisfies Legendre's necessary condition of the second order; that is, $S \geq 0$ for $\eta = \eta(u)$. The Legendre condition is called *strengthened* if the inequality is strict: $S > 0$. If a function $\eta(u)$ is an extremal, for which the strengthened Legendre condition is satisfied, and there exists no conjugate point, then $\eta(u)$ provides a local minimum to the functional (58) [11, 12].

Assume that the integrand L does not depend explicitly on the first argument: $L(u, \eta, \xi) = L(\eta, \xi)$. This assumption is satisfied in Equations (29) and (31). A differentiation of both sides of the Euler–Lagrange equation (60) with respect to u yields

$$\frac{d}{du}\left[\frac{\partial^2 L(\eta,\eta')}{\partial \eta'^2}\eta'' + \frac{\partial^2 L(\eta,\eta')}{\partial \eta' \partial \eta}\eta'\right] - \frac{\partial^2 L(\eta,\eta')}{\partial \eta' \partial \eta}\eta'' - \frac{\partial^2 L(\eta,\eta')}{\partial \eta^2}\eta' = 0 \tag{66}$$

After denoting $\xi(u) = \eta'(u)$ and making some rearrangements, one obtains

$$\frac{d}{du}\left(\frac{\partial^2 L(\eta,\eta')}{\partial \eta'^2}\xi'\right) - \left[\frac{\partial^2 L(\eta,\eta')}{\partial \eta^2} - \frac{d}{du}\left(\frac{\partial^2 L(\eta,\eta')}{\partial \eta' \partial \eta}\right)\right]\xi = 0 \tag{67}$$

One can verify by a straightforward calculations that if $\eta = \eta(u)$ is an extremal, that is, if it satisfies the Euler–Lagrange, then $\xi(u) = \eta'(u)$ satisfies the Jacobi equation. Therefore, if the derivative $\eta'(u)$ is equal to zero at an end point, say, $u = u_1$, and if the function $\eta(u)$ attains either minimum or maximum value somewhere inside the interval between u_1 and u_2, then this maximum or minimum is a conjugate point. Thus, the extremal $\eta = \eta(u)$ does not satisfy the Jacobi's condition and therefore is not a local minimum of the functional. In particular, if $\eta(u)$ is a nonconstant periodic function and the $u_2 - u_1$ is greater or equal to the period, then such an extremal is not a minimum of the functional. Indeed, since the problem is invariant with respect to a translation in u, the end point u_1 can be moved to a minimum of $\eta(u)$, so that $\eta'(u_1) = 0$. Since the length of the interval exceeds one period, the function $\eta(u)$ must attain a maximum at some $u = \widetilde{u}$, $u_1 < \widetilde{u} < u_2$. Thus, $\chi(u) = \eta'(u)$ vanishes at $u = \widetilde{u}$ and $\widetilde{u}$ is a conjugate point. Starov [30] has derived the Jacobi equation for the functional (29) assuming that the solid surface is flat.

References

1. T. Austad, B. Matre, J. Milter, A. Svareid, and L. yno, *Chemical flooding of oil reservoirs. 8. Spontaneous oil expulsion from oil- and water-wet low permeable chalk material by imbibition of aqueous surfactant solutions*, Colloids and Surfaces A: Physicochemical and Engineering Aspects **137** (1998), 117–129.
2. S. Basu and M. M. Sharma, *Measurement of critical disjoining pressure for dewetting of solid surfaces*, Journal of Colloid and Interface Science **181** (1996), 443–455.
3. M. J. Blunt, *Flow in porous media - pore-network models and multiphase flow*, Current Opinion in Colloid & Interface science **6** (2001), no. 3, 197–207.
4. M. J. Blunt and P. King, *Relative permeabilities from two- and three-dimensional pore-scale metwork modeling*, Transport in Porous Media **6** (1991), 407–433.
5. F. Brochard-Wyart, J.-M. di Meglio, D. Qur, and P.-G. de Gennes, *Spreading of nonvolatile liquids in a continuum picture*, Langmuir **7** (1991), 335–338.
6. N. V. Churaev, *On the forces of hydrophobic attraction in wetting films of aqueous solutions*, Collois and surfaces A: Physicochemical and Engineering Aspect **79** (1993), 25–31.
7. N. V. Churaev, V. M. Starov, and B. V. Derjaguin, *The shape of the transition zone between a thin film and bulk liquid and the line*

tension, Journal of Colloid and Interface Science **89** (1982), no. 1, 16–24.
8. B. V. Derjagin, *Theory of capillary condensation and related capillary effects*, Zhur. Fiz. Khim. (J. Phys. Chem.) **14** (1940), no. 2, 137–147.
9. B. V. Derjagin, N. V. Churaev, and V. M. Muller, *Surface forces*, Plenum Press, New York, 1987.
10. A. N. Frumkin, *On the wetting phenomena and attachment of bubbles*, Zhur. Fiz. Khim. (J. Phys. Chem.) **12** (1938), no. 4, 337–345.
11. I. M. Gelfand and S. V. Fomin, *Calculus of variations*, Prentice Hall, London, 1963.
12. Eduard Goursat, *Cours d'analyse mathématique*, vol. III, Gauthier-Villars, Paris, 1918.
13. A. Hiorth and G. A. Virnovsky, *Description of oil-water interface in porous rocks honouring intermolecular interactions*, Tech. Report 7001012, RF – Rogaland Reserach, Stavanger, Norway, 2005.
14. G. J. Hirasaki, *Wettability: Fundamentals and surface forces*, SPE Formation Evaluation **6** (1991), 217226.
15. Jacob N. Israelachvili, *Intermolecular and surface forces*, 2 ed., Academic Press, New York, N. Y, 1992.
16. M. Kagan and W. V. Pinczewki, *Meniscus in a narrow slit*, Journal of Colloid and Interface Science **180** (1996), 293–295.
17. _____, *Meniscus and contact angle in an eye-shaped capillary*, Journal of Colloid and Interface Science **203** (1998), 379–382.
18. _____, *Menisci in a wedge and a slit for incomplete wetting conditions*, Journal of Colloid and Interface Science **215** (1999), 196–199.
19. _____, *Menisci in a diamond-shaped capillary*, Journal of Colloid and Interface Science **230** (2000), 452–454.
20. M. Kagan, W. V. Pinczewki, and P.-E. Oren, *Two-dimensional meniscus in a wedge*, Journal of Colloid and Interface Science **170** (1995), 426–431.
21. A. R. Kovscek, H. Wong, and C. J. Radke, *A pore-level scenario for the development of mixed wettability in oil reservoirs*, AIChE J. **39** (1993), no. 6, 1072–1085.
22. S. G. Mikhlin, *Variational methods in mathematical physics*, Academtc Press, New York, 1964.
23. N. R. Morrow, H. T. Lim, and J. S. Ward, *Effect of crude-oil-induced wettability changes on oil recovery*, SPE Formation Evaluation **1** (1986), 89–95.
24. T. W. Patzek, *Verification of a complete pore network simulator of drainage and imbibition*, SPE Journal **6** (2001), no. 2, 144–156.

25. Yves Pomeau and Emmanuel Villermaux, *Two hundred years of capillary research*, Physics Today (2006), 39–44.
26. L. S. Pontryagin, *Ordinary differential equations*, Addison-Wesley, Reading, MA, 1962.
27. J. M. Schembre, G.-Q. Tang, and A. R. Kovscek, *Wettability alteration and oil recovery by water imbibition at elevated temperatures*, Journal of Petroleum Science and Engineering **52** (2006), 131–148.
28. A. Skauge, K. Spildo, L. Hiland, B. Vik, and B. Ottesen, *Experimental evidence of different intermediate wetting states*, Symposium of the Society of Core Analysts (Abu Dhabi, UAE), SCA, 2004.
29. Victor M. Starov, *Equilibrium and hysteresis contact angles*, Advances in Colloid and Interface Science **39** (1992), 147–173.
30. ———, *Nonflat equilibrium liquid shapes on flat surfaces*, Journal of Colloid and Interface Science **269** (2004), 432–441.
31. John A. Thorpe, *Elementary topics in differential geometry*, Springer, New York, 1979.
32. James W. G. Tyrrell and Phil Attard, *Images of nanobubbles on hydrophobic surfaces and their interactions*, Physical Review Letters **87** (2001), no. 17, 176104–1–176104–4.
33. Robert Weinstock, *Calculus of variations - with applications to physics and engineering*, McGrow-Hill, 1952.
34. E. K. Yeh, John Newman, and C. J. Radke, *Equilibrium configurations of liquid droplets on solid surfaces under the influence of thin-film forces Part I. Thermodynamics*, Colloids and Surfaces A: Physicochemical and Engineering Aspects **156** (1999), 137–144.
35. ———, *Equilibrium configurations of liquid droplets on solid surfaces under the influence of thin-film forces Part II. Shape calculations*, Colloids and Surfaces A: Physicochemical and Engineering Aspects **156** (1999), 525–546.
36. P. Zhang, M. T. Tweheyo, and T. Austad, *Wettability alteration and improved oil recovery by spontaneous imbibition of seawater into chalk: Impact of the potential determining ions Ca^{2+}, Mg^{2+}, and SO_4^{2-}*, Colloids and Surfaces A: Physicochem. Eng. Aspects (2007).
37. X. Zhang and P. Neogi, *Stable drop shapes under disjoining pressure: II. Multiplicity and stability*, Journal of Colloid and Interface Science **249** (2002), 141–146.
38. X. Zhang, P. Neogi, and R. M. Ybarra, *Stable drop shapes under disjoining pressure: I. A hierarchical approach and application*, Journal of Colloid and Interface Science **249** (2002), 134–140.

Lawrence Berkeley National Laboratory, 1 Cyclotron Road, MS 90R1116, Berkeley, CA 94720, USA
E-mail address: DSilin@lbl.gov

International Research Institute of Stavanger AS Postboks 8046, 4068 Stavanger, Norway